JGR Atmospheres

RESEARCH ARTICLE
10.1029/2023JD039937

Roles of Thermal Forced and Eddy-Driven Effects in the Northward Shifting of the Subtropical Westerly Jet Under Recent Climate Change

Chen Sheng[1], **Guoxiong Wu**[1,2], **Yimin Liu**[1,2], **and Bian He**[1,2]

[1]State Key Laboratory of Numerical Modeling for Atmospheric Sciences and Geophysical Fluid Dynamics (LASG), Institute of Atmospheric Physics, Chinese Academy of Sciences, Beijing, China, [2]University of Chinese Academy of Sciences, Beijing, China

Key Points:

- The thermal forced (eddy-driven) wind plays a major (secondary) role in shifting the subtropical westerly jet under recent climate change
- Thermal forced and eddy-driven effects are related to subtropical warming which mainly comes from the enhanced adiabatic sinking motion

Correspondence to:

B. He,
heb@lasg.iap.ac.cn

Citation:

Sheng, C., Wu, G., Liu, Y., & He, B. (2024). Roles of thermal forced and eddy-driven effects in the northward shifting of the subtropical westerly jet under recent climate change. *Journal of Geophysical Research: Atmospheres*, *129*, e2023JD039937. https://doi.org/10.1029/2023JD039937

Received 4 SEP 2023
Accepted 11 FEB 2024

Abstract The zonal-mean subtropical westerly jet (SWJ) in boreal winter shows a significant northward shift trend under recent climate change. Previous studies proposed thermal forcing—represented by the thermal wind associated with the temperature gradient—and the driving effect of the eddy momentum flux (EMF) convergence that leads to the eddy-driven jet as explanations for this process; however, their relative importance in influencing the SWJ shift requires further investigation. In this study, we examined the roles of thermal forced and eddy-driven jet components in the zonal-mean northward SWJ shift. We also investigated the role of Hadley circulation because its poleward boundary is related to the zonal-mean SWJ. Results suggest that thermal forced component plays a major role, while EMF-driven component plays a secondary role. Specifically, the subtropical warming, which is primarily influenced by enhanced adiabatic downward motion of the Hadley circulation, increases the meridional temperature gradient and the associated thermal wind poleward of the SWJ. It also reduces atmospheric static stability aloft and converges the EMF on the poleward side of the climatological SWJ. Enhanced meridional temperature gradient and EMF convergence on the poleward side push the SWJ northward. Results from further mathematical analysis indicate that thermal forced and eddy-driven zonal wind components account for 72% and 28% of the shift distance, respectively. In addition to elucidating the relative importance of thermal and EMF forcings, this study emphasizes the critical role of the subtropical warming driven by the intensified local descending branch of the Hadley circulation in shifting the zonal-mean SWJ.

Plain Language Summary Both the thermal forced and eddy-driven perspectives are widely used in literature to understand the northward shift of subtropical westerly jet (SWJ) under climate change. The former is related to the temperature structure, while the latter is related to the eddy momentum flux convergence. This study aims to investigate their relative importance in the northward shift of SWJ. By using a simple decomposition, this study shows that the subtropical westerly jet can be viewed as the sum of the thermal forced and eddy-driven jet components. Results suggest that the thermal forced effect plays a major role in shifting the SWJ, while the eddy-driven effect plays a secondary role. Here, it should be pointed out that the term thermal forced jet in this study refers in particular to the jet induced by the meridional gradient of temperature field, which is different from the term thermally driven jet caused by diabatic heating in some studies. This study can help readers grasp the main processes in understanding the SWJ shift, and therefore can be used in fields such as emergent constraints, that is, using the thermal forced jet to constrain the future projection of the SWJ.

1. Introduction

The tropospheric zonal flow consists of two jets with different dynamical origins: the subtropical jet and the midlatitude eddy-driven jet (Eichelberger & Hartmann, 2007). The subtropical jet is primarily influenced by the strong meridional temperature gradient (MTG) at the poleward boundary of the Hadley circulation (HC) through a thermal wind constraint, whereas the eddy-driven jet is driven by the eddy momentum flux (EMF) convergence in the midlatitudes (Vallis et al., 2004). In reality, these two jets are not always geographically separate because the polar boundary of the HC overlaps with the equatorial limit of the midlatitude baroclinic zone. As a result, the subtropical jet and eddy-driven jet often appear as one (Vallis et al., 2004), particularly during the boreal winter (Lee & Kim, 2003).

The observed subtropical westerly jet (SWJ) in Northern Hemisphere during boreal winter features a narrow and strong westerly belt with large vertical wind shears at the global zonal scale and plays an important role in the global climate and weather. Many studies, conducted by employing satellite observations (Fu & Lin, 2011; Fu et al., 2006), reanalysis data (Archer & Caldeira, 2008; Hu & Fu, 2007; Manney & Hegglin, 2018), and model simulations (Barnes & Polvani, 2013; Lorenz & DeWeaver, 2007; Vallis et al., 2015), have consistently found that the zonal-mean SWJ experiences a significant northward shift under climate change.

The causes of the long-term trend of the SWJ have been extensively investigated from both thermal forced and eddy-driven perspectives. The core of the thermal forced perspective is based on the thermal wind constraint that the change of thermal field would force the change of wind field. The underlying theoretical basis of causality in this view is that for the large-scale case, the anomalous wind filed would be mostly adjusted to the status matched with the initial thermal field anomaly through the rapid dispersion of inertia-gravity wave (i.e., atmospheric geostrophic adjustment; Holton, 2004; Yeh, 1957). This thermal forced perspective finally argues that the MTG over the subtropics would change the vertical shear of zonal wind, and therefore influence the upper-level SWJ. For instance, on the basis of satellite observations, Fu et al. (2006) indicated that a steepened MTG poleward of the SWJ favors the northward SWJ shift. Dong et al. (2022) suggested that a reduced MTG weakens the SWJ over the Eurasian sector. Yang et al. (2020, 2023) highlighted the significance of the MTG in shifting the SWJ and argued that a poleward shift of the MTG has led to the northward SWJ shift in the past 40 years. In contrast to the thermal forced perspective, the eddy-driven perspective emphasizes the role of the EMF convergence in driving the westerly jet. Early model results by Williams (1979) and Panetta and Held (1988) suggested that in the absence of a preexisting jet, eddies are capable of generating a jet through the EMF convergence. Subsequent studies further demonstrated the influential role of the EMF convergence in driving the SWJ (Chen & Held, 2007; Chen et al., 2008; Lu et al., 2014; Wu et al., 2012). For example, Lu et al. (2008) suggested that under global warming, the reduced growth of baroclinic eddies on the equatorward side of the SWJ would push the EMF convergence and the associated eddy-driven wind poleward, leading to a northward SWJ shift. The role of the HC is also discussed in the literature (e.g., Hu & Fu, 2007) because the SWJ lies at the poleward boundary of the HC.

The SWJ is influenced by different dynamical origins, and its northward shift cannot be solely attributed to a single process. As shown by Vallis et al. (2004), because thermal forced and eddy-driven components often overlap in the subtropical region, the change of the SWJ is influenced by the combined effects of thermal forced and eddy-driven processes. Nie et al. (2016) also pointed out that the response of the extratropical atmosphere to an external perturbation is a combination of a fast thermal wind adjustment and a slow eddy feedback process. Although the roles of thermal forced and eddy-driven effects have been examined separately in previous studies, the relative importance of these effects in influencing the zonal-mean northward SWJ shift remains unclear.

The primary objective of the present study is to determine the relative importance of the thermal forced and eddy-driven effects in shifting the zonal-mean SWJ during the past decades. We also examined the role of the HC because its poleward boundary is related to the SWJ. The structure of this article is as follows: Section 2 documents the data and diagnostics; Section 3 presents the features of the northward SWJ shift; Section 4 addresses the mechanism underlying the zonal-mean SWJ shift and the relative importance of thermal forced and eddy-driven effects. The summary and discussion are presented in Section 5.

2. Data and Diagnostics

2.1. Data

Monthly data, including three-dimensional winds, geopotential height, air temperature, 2-m air temperature, 10-m zonal wind, and surface pressure, were obtained from ERA5 (Hersbach et al., 2020). High-frequency ERA5 data were also used in this study. We used ERA5 daily data to measure the EMF and its convergence; ERA5 hourly data were used for the thermodynamic equation.

We also used monthly precipitation data from GPCP (Adler et al., 2018), CMAP (Xie & Arkin, 1997), and monthly outgoing longwave radiation (OLR) from the polar-orbiting satellite series of the National Oceanic and Atmospheric Administration (Liebmann & Smith, 1996).

The ERA5 data have a horizontal resolution of $1° \times 1°$. The GPCP, CMAP and OLR data have a horizontal resolution of $2.5° \times 2.5°$. The study period is 1980–2019. Boreal winter refers to the time averaged data over December to February.

2.2. Dynamical Model for Zonal Wind

For a zonally dominant flow, the horizontal momentum equation can be written as (Vallis et al., 2004):

$$\frac{du}{dt} = -\frac{\partial \phi}{\partial x} + fv + F_u \tag{1a}$$

$$0 \simeq -\frac{\partial \phi}{\partial y} - fu, \tag{1b}$$

in which (u,v) is horizontal wind; ϕ is geopotential; f is Coriolis parameter; F_u mainly represents the force of friction.

Considered the cyclic boundary conditions, the zonal-mean horizontal momentum equation in the two-dimensional incompressible case is:

$$\frac{\partial \overline{u}}{\partial t} = -\overline{\frac{\partial u' v'}{\partial y}} - r\overline{u} \tag{2a}$$

$$0 \simeq -\frac{\partial \overline{\phi}}{\partial y} - f\overline{u}, \tag{2b}$$

where $\overline{v} = 0$ is adopted because within the SWJ region the zonal mean meridional wind is weak; overbar () and prime ($'$) denote zonal mean and zonal deviation, respectively. In Equation 2a, r is a linearized inverse frictional time scale (Vallis et al., 2004).

2.2.1. Role of Eddy-Driven Effect in Changing the Surface and Upper-Level Zonal Wind

Integrating Equation 2a from the upper level to the surface over a long enough period gives:

$$\langle r\overline{u} \rangle \simeq \left\langle -\overline{\frac{\partial u' v'}{\partial y}} \right\rangle, \tag{3}$$

where $\langle\rangle$represents the vertical integration. Because the friction peaks at the surface, Equation 3 leads to a scaling law between the zonal-mean surface westerly ($\overline{u}_s$) and the vertically integrated EMF convergence:

$$\overline{u}_s \propto \left\langle -\overline{\frac{\partial u' v'}{\partial y}} \right\rangle. \tag{4}$$

Equation 4 suggests an *eddy-driven effect*; *the zonal-mean surface westerly ($\overline{u}_s$) is driven by the vertically integrated zonal-mean EMF convergence*. That is mentioned in "downward control" mechanism (Haynes et al., 1991), which suggested that the upper-level eddy can drive the surface westerly.

At the upper level, friction is negligible Equation 2a approximates a balance between the acceleration of zonal wind and EMF convergence (Held, 2000):

$$\frac{\partial \overline{u}}{\partial t} \simeq -\overline{\frac{\partial u' v'}{\partial y}}. \tag{5}$$

Equation 5 suggests that at the upper level, EMF convergence (divergence) could accelerate (decelerate) the upper-level zonal wind. However, the force of the EMF convergence in Equation 5 corresponds to the acceleration of zonal wind rather than the zonal wind itself, and a higher acceleration does not imply a higher velocity. Therefore, Equation 5 is not appropriate for the examination of how the variation of the EMF convergence changes the upper-level SWJ. This is in accordance with Held (2000) who stressed that it is a common mistake to refer to EMF maintenance of upper-level winds, which are mostly controlled by vertical shears.

2.2.2. Role of Thermal Forced Effect in Influencing the SWJ

In this study, the upper-level SWJ is regarded as the sum of the eddy-driven surface westerly $\overline{u}_s$ and the vertical shear $\overline{u}_v(p)$:

$$\overline{u}(p) = \overline{u}_s + \overline{u}_v(p), \tag{6}$$

in which:

$$\overline{u}_v(p) = \int_{ps}^{p} \frac{\partial \overline{u}}{\partial p} dp. \tag{7}$$

Equation 7 can be further decomposed into the geostrophic component $\left\langle \frac{\partial \overline{u}_g}{\partial p} \right\rangle$ and the residual ageostrophic component $\overline{u}_a$:

$$\overline{u}_v(p) = \int_{ps}^{p} \frac{\partial \overline{u}_g}{\partial p} dp + \overline{u}_a(p). \tag{8}$$

For the ageostrophic component $\overline{u}_a$, a comparison between Equations 2a and 2b suggests that the $\overline{u}_a$ can be driven by the EMF convergence, especially at the upper level where the friction is small. For the geostrophic component $\left\langle \frac{\partial \overline{u}_g}{\partial p} \right\rangle$, adopting the thermal wind constraint gives:

$$\int_{ps}^{p} \frac{\partial \overline{u}_g}{\partial p} dp = \int_{ps}^{p} \frac{R}{fp} \frac{\partial \overline{T}}{\partial y} dp = \overline{u}_T(p), \tag{9}$$

in which R is the ideal gas constant, and $\overline{T}$ is zonal-mean temperature. The $\overline{u}_T$ *marks the zonal wind component forced by the meridional thermal structure*, that is, *thermal forced zonal wind*.

2.2.3. Decomposition of the SWJ Into the Thermal Forced and Eddy-Driven Components

Substituting Equations 8 and 9 into Equation 6, we have:

$$\begin{cases} \overline{u}(p) = + \underbrace{\overline{u}_T(p)}_{\text{thermal forced}} + \underbrace{\overline{u}_e(p)}_{\text{eddy-driven}} \\ \overline{u}_e(p) = \overline{u}_s + \overline{u}_a(p) \end{cases} \tag{10}$$

Equation 10 suggests that the zonal-mean SWJ is the sum of thermal forced zonal wind ($\overline{u}_T$) and eddy-driven zonal wind ($\overline{u}_e$), where $\overline{u}_e$ includes the eddy-driven $\overline{u}_s$ and $\overline{u}_a$. Diagnosing Equation 10 gives the contribution of each component. In the diagnosing process, the surface westerly $\overline{u}_s$ can be obtained directly from the reanalysis data, and the $\overline{u}_T$ can be obtained by vertically integrating MTG in Equation 9. However, because the eddy-driven $\overline{u}_a$ is difficult to be obtained directly or calculated from reanalysis data, it is represented by the residual in Equation 10 in this study. Equation 10 is somewhat like the idea of Waugh et al. (2018) and Davis and Birner (2016, 2017), in which they obtain the subtropical jet by subtracting the low-level zonal wind (850-hPa zonal wind in the former and surface zonal wind in the latter) from raw zonal wind. In comparation of Waugh et al. (2018) and Davis and Birner (2016, 2017), the present study adopts a more rigorous mathematical derivation and further eliminate the ageostrophic component $\overline{u}_a$, which could be driven by EMF convergence, from the subtropical jet.

2.3. Thermodynamic Equation

The thermodynamic equation is:

$$\frac{\partial \theta}{\partial t} = -u\frac{\partial \theta}{\partial x} - v\frac{\partial \theta}{\partial y} - \omega\frac{\partial \theta}{\partial p} + \dot{\theta}. \tag{11}$$

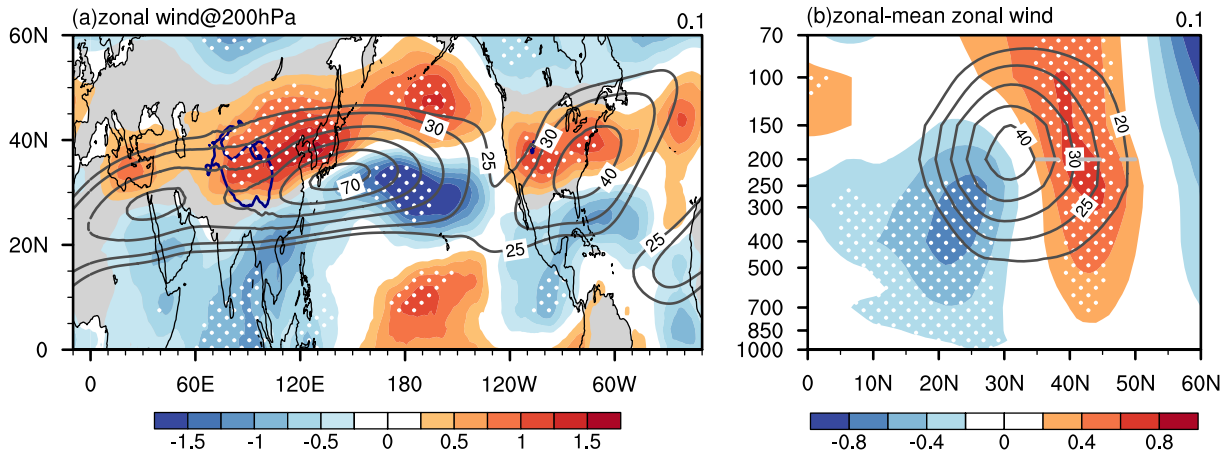

Figure 1. (a) Climatological mean (contour; unit: m s^{-1}) and trend (shading; unit: m s^{-1} $decade^{-1}$) of zonal wind at 200 hPa during boreal winter. (b) Cross section of climatological mean (contour; unit: m s^{-1}) and trend (shading; unit: m s^{-1} $decade^{-1}$) of zonal-mean zonal wind during boreal winter. Areas exceeding a significance level of 0.1 are indicated by white dots.

where θ is potential temperature; ω is vertical wind; $\dot{\theta}$ is diabatic heating; $-u\frac{\partial\theta}{\partial x}-v\frac{\partial\theta}{\partial y}$ is horizontal advection of potential temperature; $-\omega\frac{\partial\theta}{\partial p}$ is vertical advection of potential temperature. Substituting $\theta=T\left(p_0/p\right)^{\kappa}$ into $-\omega\frac{\partial\theta}{\partial p}$ gives:

$$-\omega\frac{\partial\theta}{\partial p}=-\omega\frac{\partial T}{\partial p}\left(\frac{p_0}{p}\right)^{\kappa}+\omega\frac{RT}{C_p p}\left(\frac{p_0}{p}\right)^{\kappa}, \tag{12}$$

in which C_p is specific heat at constant pressure and $\kappa=R/C_p$. According to Equation 12, the vertical advection of potential temperature includes the advective process (first term in the right-hand side) and the adiabatic process (second term in the right-hand side) of temperature.

3. Features of Northward Shift of the Zonal-Mean SWJ

Figure 1 shows the three-dimensional structure of the climatological mean state and the linear trend of the zonal wind. Climatologically, there is a strong SWJ belt over the subtropics (Figure 1a). In the SWJ, there are two centers of high winds; one extends to the east of East Asia and reaches a maximum of 70 m s^{-1}; the other extends over North America and reaches 40 m s^{-1}. Along the edges of the climatological SWJ is a remarkable dipole pattern in the trend of the zonal wind (shading in Figure 1a); the positive pole is on the poleward side and the negative pole is on the equatorward side. These features are also clear in the cross section (Figure 1b). In the cross section of zonal-mean zonal wind (Figure 1b), the SWJ is centered at 30°N; it peaks at 200 hPa with maximum speeds exceeding 40 m s^{-1}. The equatorward side of the SWJ shows a negative trend while the poleward side shows a positive trend. Although the magnitudes of the trends (Figure 1) are small compared with the climatological means, the trends are statistically significant with p-values of less than 0.1. Overall, the significant dipole pattern in Figure 1 indicates a zonal-mean northward SWJ shift.

Empirical orthogonal function (EOF) analysis provides additional evidence for the northward shift of the zonal-mean SWJ. Figure 2 shows the first two EOFs of zonal-mean zonal wind and the corresponding principal component time series. The EOF1 (Figure 2a) represents a uniform mode of variation in the zonal-mean SWJ centered at 30°N and explains 40.7% of the total variance. The principal component of EOF1 (Figure 2b) has prominent interannual variability, which indicates pulsing of the intensity of the zonal-mean SWJ. However, the linear trend is statistically insignificant with a p-value of 0.8. The EOF2 (Figure 2c) captures a dipole mode in the variation of the zonal-mean SWJ. It explains 25.6% of the total variance. The principal component of EOF2 (Figure 2d) has a statistically significant positive trend with a p-value of less than 0.05. This trend implies a

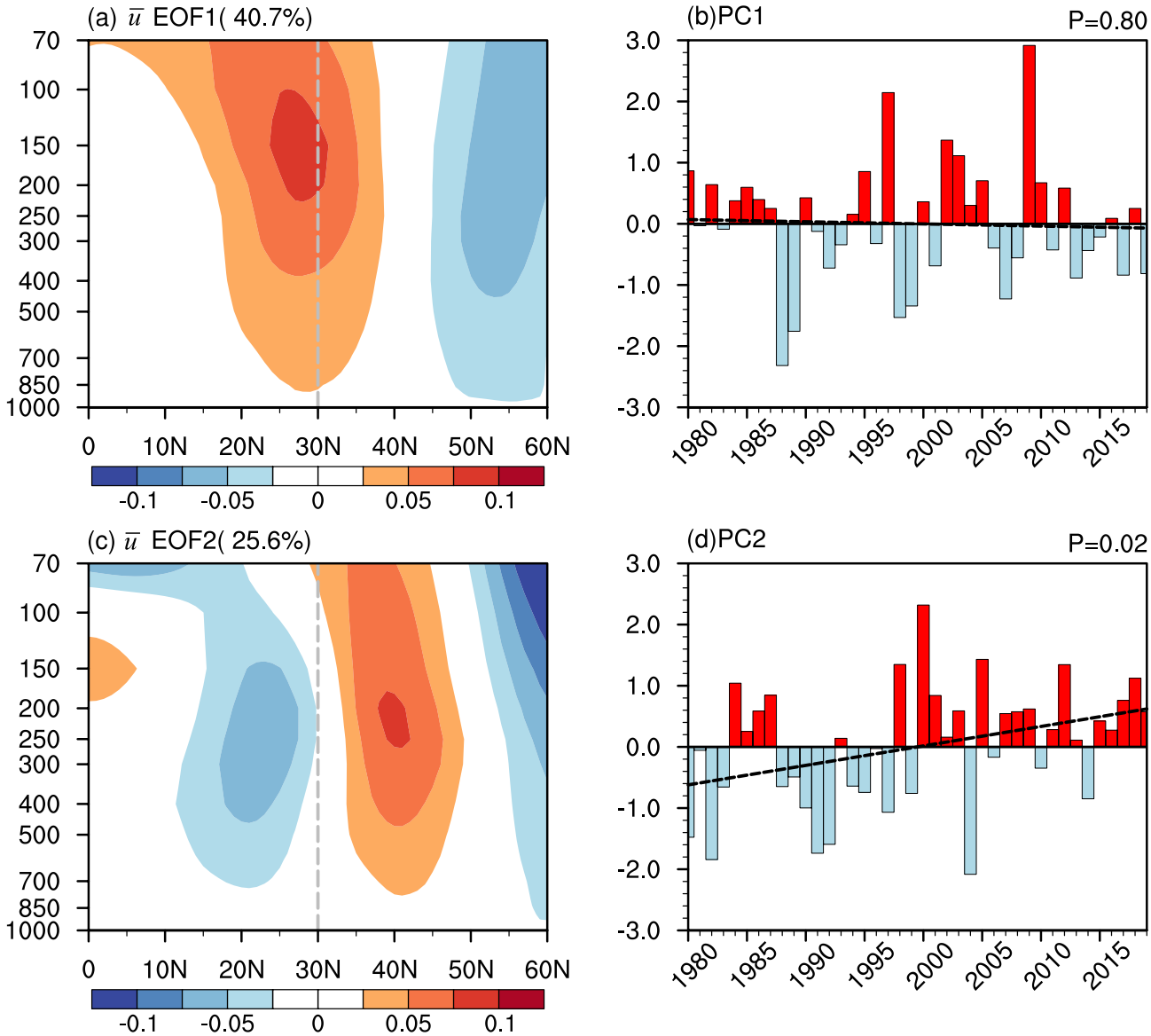

Figure 2. (a) Cross section of the EOF1 mode and (b) the corresponding principal component time series of zonal-mean zonal wind during boreal winter. (c), (d) same as (a), (b), but for EOF2 mode. Black dashed line indicates the linear trend.

decreased speed on the equatorward side and an increased speed on the poleward side of the zonal-mean SWJ. Therefore, EOF2 captures a notable northward shift of the zonal-mean SWJ.

To quantitively measure the distance of the zonal-mean northward SWJ shift, Figure 3 presents the time series of the latitude of the SWJ axis. We defined the latitude of the SWJ axis as the mean latitude at which zonal-mean 200-hPa SWJ exceeds 25 m s^{-1}. There is a clear positive trend of 0.38° $decade^{-1}$ in the latitude of the zonal-mean SWJ axis over the study period (Figure 3). Although this trend has a p-value of less than 0.05, it is smaller than the horizontal resolution of the data used in this study. Therefore, further theoretical analysis of the northward shift distance is needed.

Considering that the linear trend of the SWJ is much smaller than its climatological mean value (Figure 1b), it can be assumed that the zonal-mean SWJ maintains its shape during its northward shift. That is to say, it can be assumed that the SWJ at latitude y_0 is moved from $y_0 - \delta y$ where δy is the distance of the northward shift. Therefore, the relationship between the linear trend $\delta\overline{u}$ and shift distance δy is $\delta\overline{u} = \overline{u}(y_0 - \delta y) - \overline{u}(y_0) \simeq -\delta y \partial\overline{u}/\partial y$ (Kushner et al., 2001) and can be further expressed as:

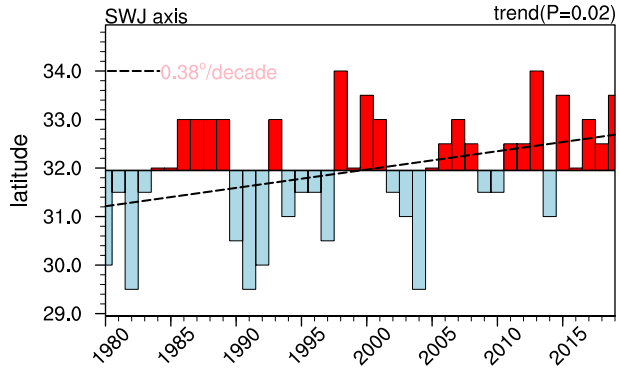

Figure 3. Time series of the latitude of the SWJ axis during boreal winter. Black dashed line indicates the linear trend.

$$\delta y \simeq -\delta\overline{u}/\frac{\partial\overline{u}}{\partial y}. \quad (13)$$

In Equation 13, by using the linear trend and the climatological mean zonal-mean zonal wind at 200 hPa averaged over 35°–50°N (gray dashed line in Figure 1b), we calculated the northward SWJ shift distance. This results in a value of δy of 0.36° decade^{-1}, which is very close to the value obtained from Figure 3 (0.38° decade^{-1}). This result is also comparable with that in Allen et al. (2012) in which the latitude shift of the tropospheric zonal wind maxima is evaluated.

4. Mechanism

The results in Section 3 indicate a significant northward shift trend of the zonal-mean SWJ. In Section 4, we investigate the mechanism responsible for this shift, the relative importance of thermal forced and eddy-driven effects in influencing the shift, and the role of the HC.

4.1. Role of HC Expansion

The zonal-mean SWJ lies at the poleward boundary of the HC (Eichelberger & Hartmann, 2007). We used three distinct criteria to measure the trend of the latitude of the HC poleward boundary in the Northern Hemisphere and found that trends vary with criterion (Figure 4). Using the latitude at which the 500-hPa meridional stream function (MSF) reaches zero as the latitude of the HC boundary (Figure 4a; Kang & Lu, 2012), we found a negative trend that is statistically insignificant ($p = 0.34$); this indicates slight shrinkage of the HC. We also defined the HC boundary by the latitude at which the 500-hPa MSF drops to 10% of its maximum magnitude (Figure 4b; Kang et al., 2013). Following this criterion, the HC boundary has a positive trend that is statistically insignificant, which suggests a very weak expansion of the HC. These results align with the findings of Hu and Fu (2007) and Hu et al. (2018), which show no significant trend in the HC extent during boreal winter. However, using the latitude at which the surface zonal wind changes its sign as the latitude of the HC boundary (Figure 4c; Vallis et al., 2015), we found a statistically significant positive trend with a p-value of less than 0.05. This suggests a northward expansion of the low-level HC boundary and the associated surface easterly. Although the low-level HC boundary exhibits a significant trend of northward shift (Figure 4c), the upper-level HC boundary, which is directly tied to the upper-level SWJ, remains almost unchanged. Consequently, the shift of the HC boundary cannot account for the zonal-mean northward SWJ shift. These results are similar to those of Kushner et al. (2001), which indicate a separation of the HC poleward boundary from the SWJ in the Southern Hemisphere under global warming. Recently, Menzel et al. (2019) further found that the location of subtropical jet does not

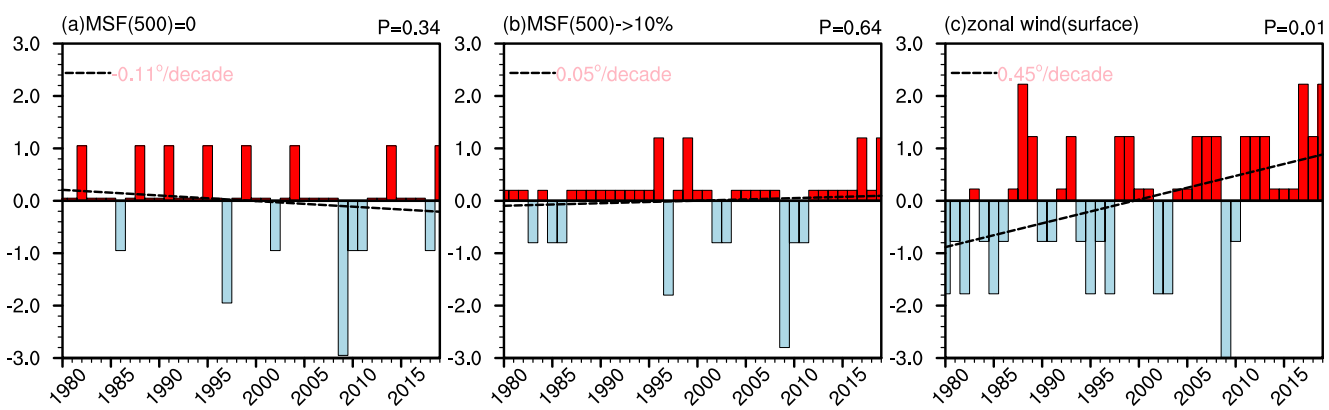

Figure 4. Latitude of the boreal winter HC poleward boundary as defined by the latitude at which the (a) 500-hPa meridional stream function (MSF) reaches zero, (b) 500-hPa MSF drops to 10% of its maximum magnitude, and (c) surface zonal wind changes its sign. Black dashed line indicates the linear trend.

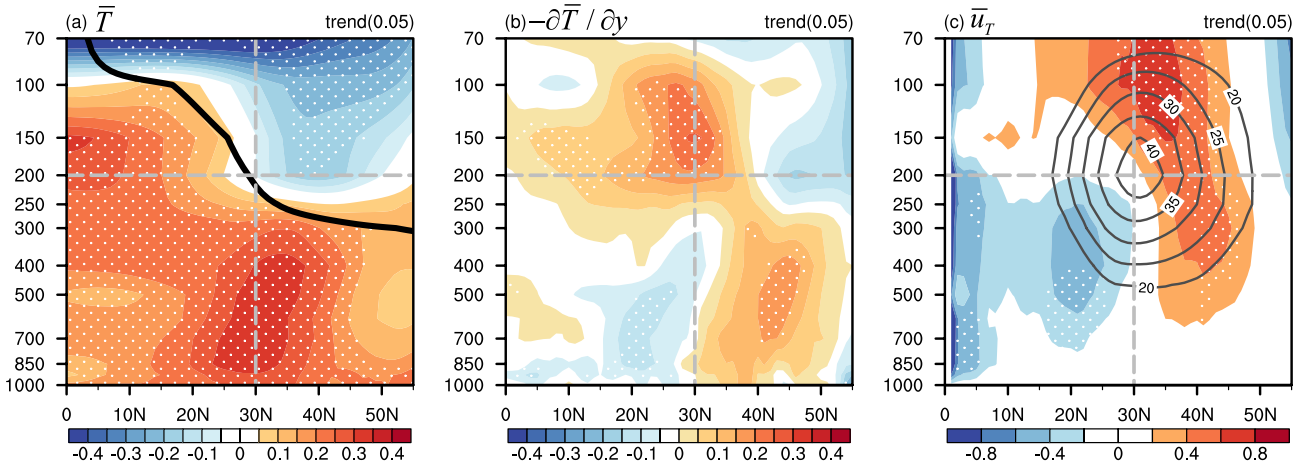

Figure 5. Cross sections of linear trends during boreal winter of (a) zonal-mean air temperature, (b) zonal-mean meridional temperature gradient, and (c) thermal forced zonal wind. Black line in (a) indicates 2 PVU. Contours in (c) indicate climatological zonal-mean zonal wind during boreal winter. Areas exceeding a significance level of 0.05 are indicated by white dots.

covary interannually with the latitude of the poleward HC edge in the models from Coupled Model Intercomparison Project Phase 5.

4.2. Role of Thermal Forced Effect

Figure 5 presents the cross sections of the linear trends of zonal-mean air temperature (Figure 5a), MTG (Figure 5b), and the thermal forced zonal wind $\overline{u}_T$ (Figure 5c). In Figure 5a, the tropopause represented by 2 PVU (1 PVU = 10^{-6} K m^2 kg^{-1} s^{-1}) is marked by the black bold line. Figure 5a features a clear pattern of stratospheric cooling and tropospheric warming. This pattern leads to more unstable stratification and a nonexpanding HC (Figures 4a and 4b) because the HC extent is proportional to the static stability which is suggested by a scaling law (Held, 2000). Figure 5b shows the cross section of the linear trend of MTG that corresponds to the zonal-mean air temperature represented in Figure 5a. A dipole mode and a single positive center are evident below and above 200 hPa, respectively. This dipole mode of MTG results from the enhanced subtropical warming, while the positive center of MTG results from the thermal contrast between the tropical tropospheric warming and subtropical stratospheric cooling.

Figure 5c presents the trend of thermal forced zonal wind $\overline{u}_T$ by vertically integrating MTG (Figure 5b). Results to the south of 10° N should be ignored because the quasi-geostrophic constraint is inapplicable in the tropics. To the north of 10° N, the trend of thermal forced zonal wind $\overline{u}_T$ (Figure 5c) bears a strong resemblance to the linear trend of raw zonal-mean zonal wind (Figure 1b), suggesting that the thermal wind constraint plays an important role in the zonal-mean northward SWJ shift. Furthermore, through the thermal wind constraint (Equation 9), the strengthened (reduced) MTG is associated with the strengthened (reduced) thermal forced zonal wind $\overline{u}_T$. Therefore, the stratospheric MTG (Figure 5b) primarily contributes to an increase in the stratospheric thermal forced zonal wind $\overline{u}_T$ (Figure 5c), while the tropospheric dipole MTG (Figure 5b) leads to the dipole pattern in the thermal forced zonal wind $\overline{u}_T$ (Figure 5c). On the basis of these results, we argue that tropospheric subtropical warming (Figure 5a), which leads to the tropospheric dipole MTG (Figure 5b), is important for the northward shift of the zonal-mean SWJ.

To further illustrate the formation of the subtropical warming, Figure 6a shows the climatological mean (contour) and linear trend (shading) of the MSF. Blue and red arrows indicate the trend of upward and downward motion, respectively. The black box in Figure 6a marks the region of major subtropical warming in Figure 5a. Consistent with Figures 4a and 4b, Figure 6a indicates no trend in the position of the HC boundary in the subtropical region. However, the downward motion is enhanced over the subtropical region (vectors in Figure 6a), which is consistent with that the trend of MSF sharps the meridional gradient of subtropical climatological mean MSF (Figure 6a). Since the Ferrel cell is an indirect cell, it is clear that the vectors of the Ferrel cell are weak than that of the HC (Figure 6a). Therefore, the enhanced downward motion is mainly contributed by the enhanced HC

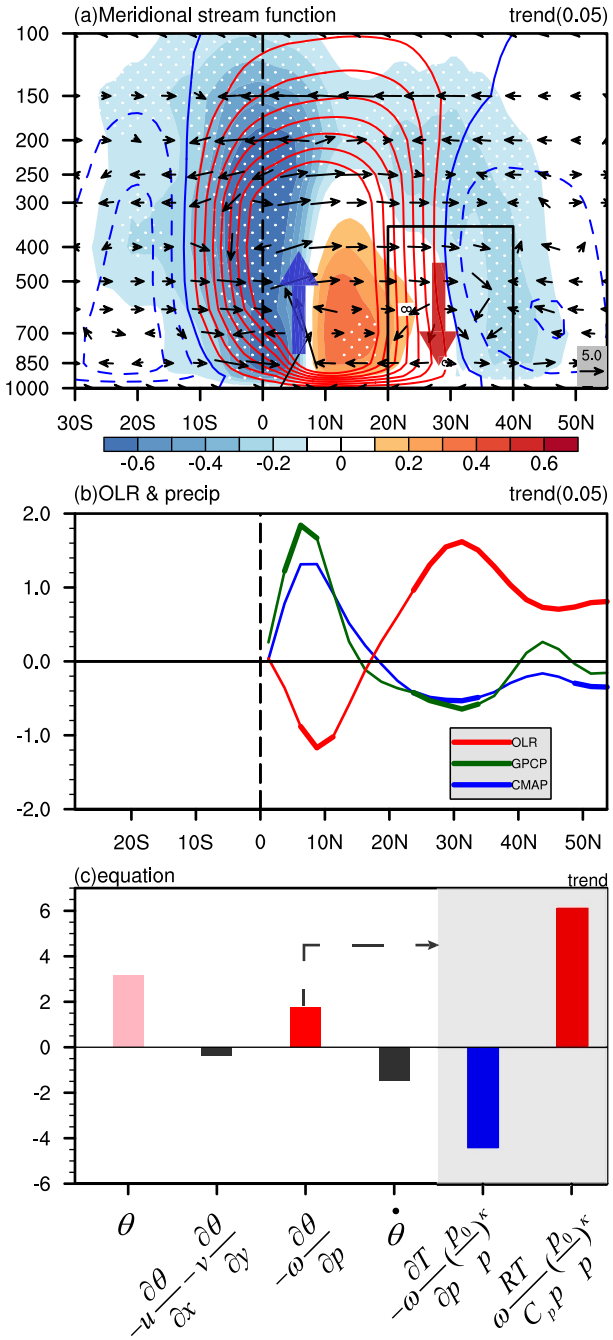

Figure 6. (a) Climatological mean (contour; unit: 10^{10} kg s^{-1}) and trend (shading; unit: 10^{10} kg s^{-1} decade^{-1}) of the MSF during boreal winter. Vectors indicate the trend of meridional circulation. Blue and red arrows indicate the trend of upward and downward motion, respectively. Areas exceeding a significance level of 0.05 are indicated by white dots. (b) Trends of zonal-mean OLR (red curve; unit: W m^{-2} decade^{-1}) and zonal-mean precipitation (unit: 10^{-1} mm day^{-1} decade^{-1}) from GPCP (green curve) and CMPA (blue curve) during boreal winter. Thick lines indicate $p < 0.05$. (c) Trends of the potential temperature (pink bar) and the right-hand side terms (other bars) of thermodynamic equation (Equations 11 and 12) averaged over the black box in (a) during boreal winter. Unit for pink bar is 10^{-1} K decade^{-1}. Units for the other bars are 10^{-7} K s^{-1} decade^{-1}.

descending branch. Because the HC is non-divergent and is predominately thermally driven (Eichelberger & Hartmann, 2007), we can see the intensified HC descending branch corresponds to a enhanced equatorial ascending motion (Figure 6a) and latent heat release (Figure 6b). There is a close agreement between the trend of vertical motion (Figure 6a) and that of zonal-mean precipitation and OLR (Figure 6b). A descending motion over the subtropical region leads to an increasing OLR and decreasing precipitation, while an ascending motion on the equatorward side leads to a decreasing OLR and increasing precipitation (Figure 6b).

Figure 6c shows the diagnostic result of the thermodynamic equation (Equation 11) using hourly data. The diagnostic result is averaged over the region of subtropical warming in the black box in Figure 6a. Because the dominant motion in the region of subtropical warming is vertical motion associated with the HC, the linear trend of averaged horizontal potential temperature advection is expected to be small (Figure 6c). The diabatic heating $\dot{\theta}$ (Figure 6c) shows a negative trend, which is mainly attributed to the increasing OLR and reduced latent heating due to the decreasing precipitation (Figure 6b). As a result, the subtropical warming is largely determined by the enhanced vertical advection of potential temperature (Figure 6c). The vertical advection of potential temperature includes the advective and adiabatic processes of temperature (Equation 12). Further decomposition of the result suggests that the adiabatic warming induced by the enhanced descending motion plays a major role in driving the subtropical warming (Figure 6c). These results indicate that (a) although there is no significant trend in the extent of the HC, the intensity of the descending branch of the HC is enhanced; (b) the atmospheric dynamic process, that is, the adiabatic warming of the HC's descending branch, mainly contributes to the formation of the subtropical warming (Figure 6c) while diabatic processes, such as, the radiation and latent heating release (Figure 6b) contribute less.

4.3. Role of Eddy-Driven effect—EMF Convergence Forcing

In addition to the thermal forced zonal wind $\overline{u}_T$, Equation 10 suggests that the zonal-mean zonal wind is also influenced by the eddy-driven effect. Figure 7 shows the climatological mean (left column) and the linear trend (right column) associated with the EMF and surface westerly. In Figure 7a, the zonal-mean EMF maximum and SWJ almost overlap, suggesting a prominent northward transport of eddy momentum in the SWJ. This structure in Figure 7a is consistent with the findings of Vallis et al. (2015). In Figure 7c, the zonal-mean EMF convergence shows a dipole structure that diverges on the equatorward side and converges on the poleward side. Because the convergence (divergence) of EMF tends to increase (decrease) the zonal-mean SWJ (Equation 5), we can see that the zonal-mean SWJ (contour) on the poleward side is stronger than that on the equatorward side (Figure 7c). In Figure 7e, there is a close agreement between the signs of vertically integrated zonal-mean EMF convergence (line) and those of the surface zonal wind (shading), implying an eddy-driven effect on the zonal-mean surface westerly (Equation 4). A similar pattern can also be seen in the trends (Figures 7b, 7d, and 7f). The zonal-mean EMF (Figure 7b) is enhanced relative to climatological means (Figure 7a). This is mainly because that the critical shear ($U_c \propto \partial ln\theta/\partial z$) and critical wavelength ($L_c \propto \sqrt{-\partial \ln \theta/\partial p}$) for baroclinic instability increase with the static stability (Holton, 2004; Phillips, 1954; Vallis et al., 2015). The unstable stratification (i.e., decreased static stability; Figure 5a), which is caused by the subtropical warming, would lead to a

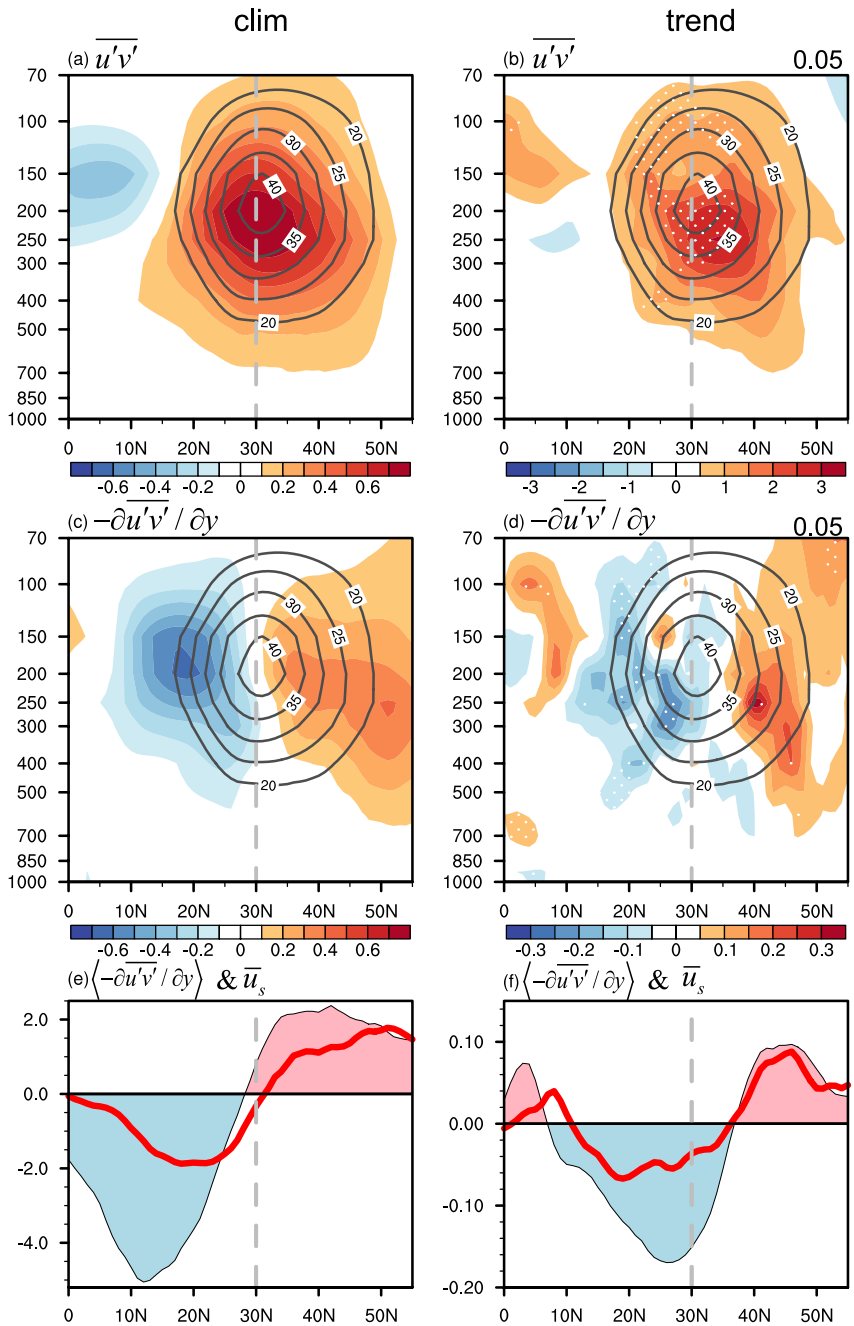

Figure 7. Climatological mean of zonal-mean (a) EMF, (c) EMF convergence, (e) vertically integrated EMF convergence (red curve), and surface zonal wind (shading) during boreal winter. (b), (d) and (f) same as (a), (c) and (e), but for trend. Contours in (a–d) indicate climatological zonal-mean zonal wind during boreal winter. Areas exceeding a significance level of 0.05 are indicated by white dots.

decreased critical wavelength and a decreased critical shear so that more wave become baroclinic instability and the resultant eddy momentum transport is enhanced. The zonal-mean EMF convergence trend (Figure 7d) favors an increased acceleration of speed on the poleward side of the zonal-mean SWJ, and therefore contributes to a zonal-mean northward SWJ shift. In Figure 7f, there is a close agreement between the signs of vertically integrated zonal-mean EMF convergence (line) and those of the eddy-driven surface zonal wind (shading). Such a subtropical dipole pattern (Figure 7f) of eddy-driven surface zonal wind favors the zonal-mean northward SWJ shift (Equation 10). These results suggest that the eddy-driven effect tends to increase the upper-level zonal-mean

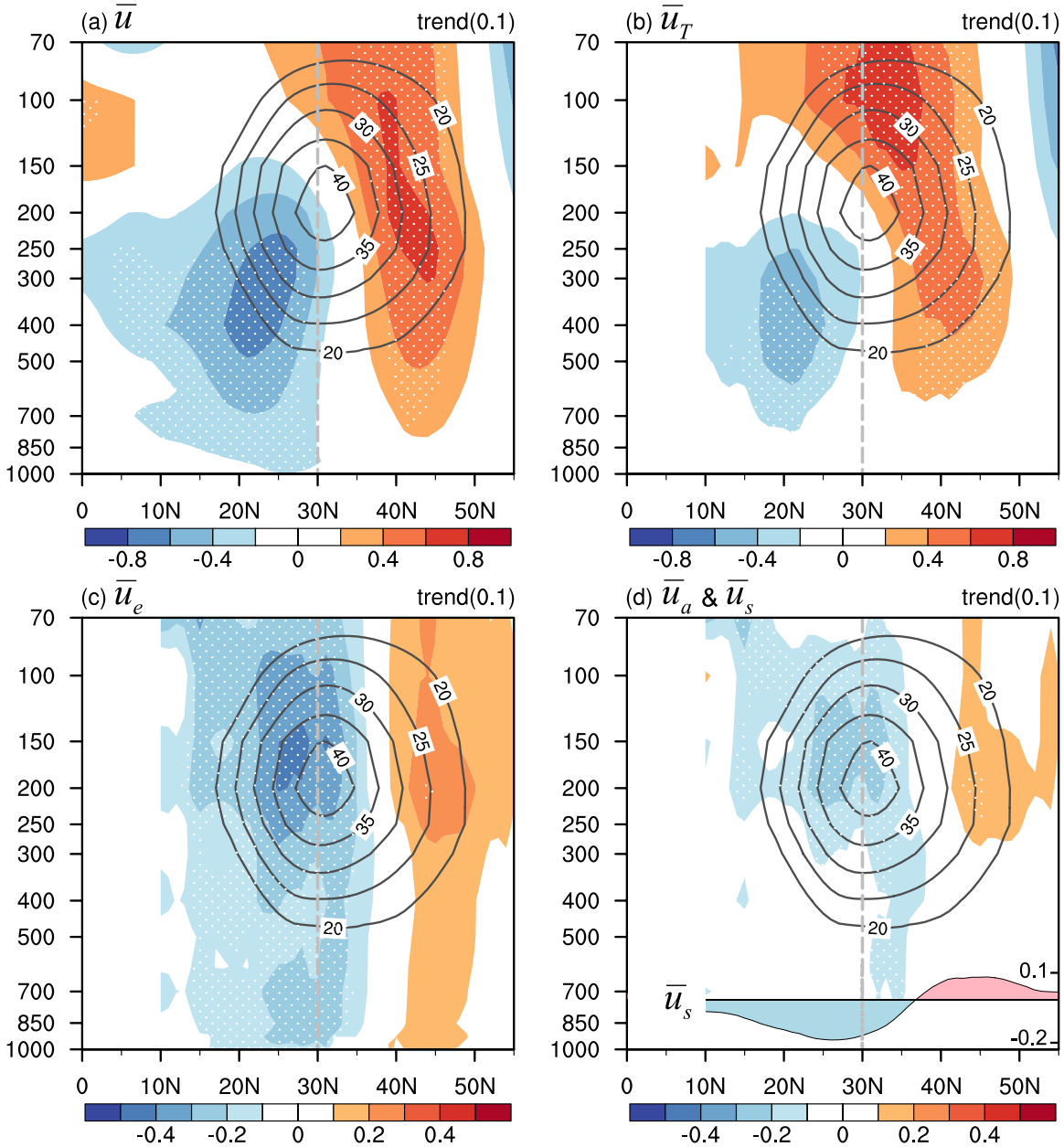

Figure 8. Cross sections of linear trends during boreal winter of zonal-mean (a) zonal wind, (b) thermal forced zonal wind, (c) eddy-driven zonal wind, and (d) ageostrophic zonal wind (shading) and eddy-driven surface zonal wind (bottom curve). In (a–d), contours indicate climatological zonal-mean zonal wind (unit: m s^{-1}) during boreal winter. Areas exceeding a significance level of 0.1 are indicated by white dots In (b–d), results to the south of 10° N in (b–d) are omitted. The eddy-driven surface zonal wind (curve in graph; unit: m s^{-1} $decade^{-1}$) in (d) is the same as that in Figure 7d.

zonal wind and drive the zonal-mean surface westerly poleward of the climatological zonal-mean SWJ; therefore, it also plays a role in driving the northward shift of zonal-mean SWJ via the EMF convergence.

4.4. Relative Contributions of Thermal Forced and Eddy-Driven Effect to the Zonal-Mean Northward SWJ Shift

To facilitate a comparison of the relative contributions of thermal forced and eddy-driven zonal wind to the zonal-mean northward SWJ shift, the trends of raw zonal-mean zonal wind (Figures 1b and 8a), thermal forced zonal wind $\overline{u}_T$ (Figures 5c and 8b), and eddy-driven zonal wind $\overline{u}_e$ (Figure 8c) are shown again in Figure 8. There is a close agreement between the linear trend of thermal forced zonal wind $\overline{u}_T$ (Figure 8b) and that of the raw zonal-

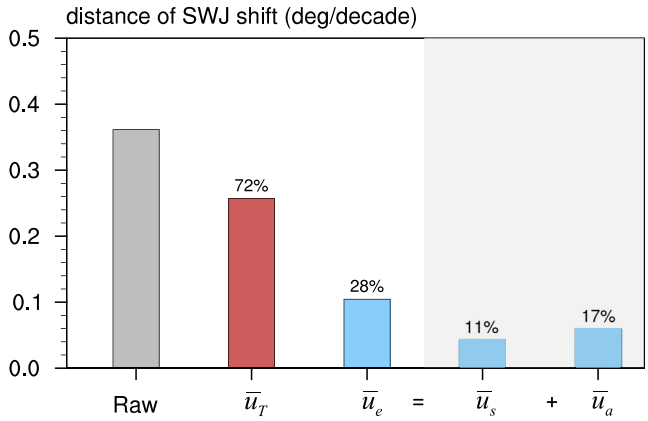

Figure 9. Contribution of thermal forced zonal wind (red bar) and eddy-driven zonal wind (blue bar with black outline) and its components (blue bars with no outline) to the distance of zonal-mean northward SWJ shift (gray bar) during boreal winter. The unit of the vertical axis is ° decade^{-1}.

mean zonal wind (Figure 8a), suggesting a dominant contribution of thermal forced zonal wind $\overline{u}_T$ to the zonal-mean northward SWJ shift. The eddy-driven zonal wind $\overline{u}_e$ (Figure 8c), which often exhibits an equivalent barotropic structure (Nie et al., 2016), also shows a clear dipole pattern. However, the linear trends of eddy-driven zonal wind $\overline{u}_e$ and its components (Figure 8d) are smaller than the trend of thermal forced zonal wind $\overline{u}_T$ (Figure 8b). These results indicate that the zonal-mean northward SWJ shift is primarily governed by the thermal forced effect while the eddy-driven effect is a secondary driver.

We substituted the linear trends of raw zonal-mean zonal wind, thermal forced zonal wind $\overline{u}_T$, and eddy-driven zonal wind $\overline{u}_e$ and its components (i.e., $\overline{u}_s$ and $\overline{u}_a$) averaged over 35°–50°N (gray dashed line in Figure 1b) into the numerator of Equation 13 to calculate the distance of zonal-mean northward SWJ shift induced by thermal forced and eddy-driven effects. Results (Figure 9) suggest that the distance induced by thermal forced zonal wind $\overline{u}_T$ (red bar) and eddy-driven zonal wind $\overline{u}_e$ (blue bar with black outline) are approximately 0.26° and 0.1° decade^{-1}, accounting for 72% and 28% of the distance of the zonal-mean northward SWJ shift (gray bar; 0.36° decade^{-1}), respectively. The shift distance induced by eddy-driven zonal wind $\overline{u}_e$ is composed of contributions from the eddy-driven surface westerly $\overline{u}_s$ and eddy-driven upper-level zonal wind $\overline{u}_a$; $\overline{u}_s$ and $\overline{u}_a$ account for 11% and 17% of the shift distance, respectively. These results further confirm the dominant role of the thermal forced effect and the secondary role of the eddy-driven effect in driving the zonal-mean northward SWJ shift.

5. Summary and Discussion

5.1. Summary

The boreal winter zonal-mean SWJ shows a significant northward shift trend under recent climate change (1980–2019). Previous studies have proposed thermal forcing and EMF convergence as explanations for this shift, but the relative importance of the two is not well understood. In this study, we conducted a theoretical analysis and identified the thermal forced jet and eddy-driven jet as two components of the zonal-mean SWJ. We investigated the relative contributions of the thermal forced jet and the eddy-driven jet to the zonal-mean northward SWJ shift. We also examined the role of the HC because the poleward boundary of the HC is related to the SWJ. The mechanism responsible for the zonal-mean northward SWJ shift is shown schematically in Figure 10. Main conclusions drawn from the present study are as follows.

1. Reanalysis data and theoretical analysis suggest the zonal-mean northward SWJ shift with approximately 0.36° decade^{-1}. This trend cannot be explained by HC expansion because the shift of the HC poleward boundary is insignificant in boreal winter. Although the HC extent shows no significant trend, the intensity of the descending branch of the HC is enhanced (Figure 10). According to the results of our thermodynamic equation analysis, the enhanced adiabatic warming of the descending branch of the HC in association with the intensified equatorial convection, rather than advection and radiation processes, contributes to the significant subtropical warming, which plays a critical role in shaping the observed zonal-mean northward SWJ shift.
2. The enhanced subtropical warming increases (decreases) the MTG poleward (equatorward) of the zonal-mean SWJ. This dipole MTG pattern results in an increasing (a decreasing) of thermal forced zonal wind poleward (equatorward) of the zonal-mean SWJ, thereby contributing to a significant zonal-mean northward SWJ shift (Figure 10). The thermal forced zonal wind accounts for approximately 72% of the zonal-mean northward SWJ shift, which corresponds to a trend of 0.26° decade^{-1}. Therefore, we conclude that the thermal forced effect plays a major role in driving the zonal-mean northward SWJ shift.
3. The enhanced subtropical warming also leads to a decrease in atmospheric static stability aloft. The induced unstable stratification intensifies the northward transport of eddy momentum over the SWJ center through decreasing the critical shear and critical wavelength, resulting in an EMF convergence (divergence) poleward (equatorward) of the zonal-mean SWJ (Figure 10). Eddy-driven zonal wind thus also leads to a zonal-mean northward SWJ shift. The eddy-driven zonal wind accounts for approximately 28% of the zonal-mean

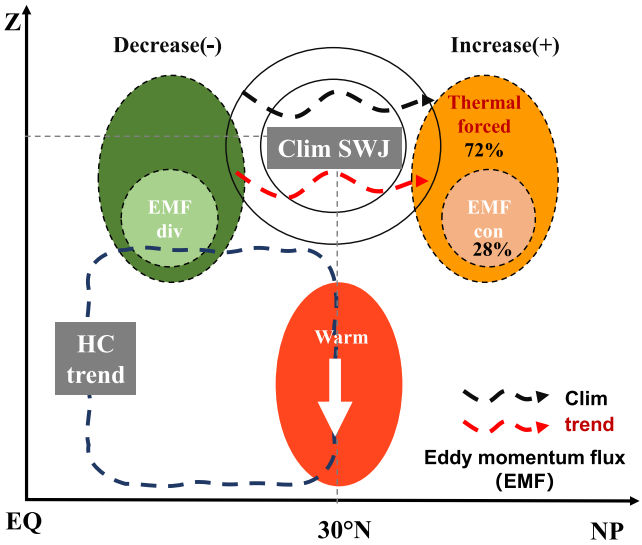

Figure 10. Schematic of the mechanism responsible for the zonal-mean northward SWJ shift during boreal winter. The solid (dashed) ovals indicate the climatological (trend of) SWJ. The black (red) curved vector indicates climatological (trend of) EMF. The white vector indicates the trend of vertical motion. The red oval indicates the enhanced subtropical warming. The dashed quadrilateral indicates the trend of HC; EQ and NP indicate the equator and North Pole, respectively.

northward SWJ shift, which corresponds to a trend of 0.11° decade^{-1}. Therefore, we conclude that the eddy-driven effect plays a secondary role in driving the zonal-mean SWJ shift.

5.2. Discussion

The eddy heat flux may also play a role but is not emphasized yet in this study. There are two reasons. Firstly, the eddy heat flux peaks at mid-high latitudes, while within the SWJ region around 30°N the eddy heat flux is very weak (Chen & Huang, 2002). Therefore, the direct forcing of eddy heat flux, embedded in Eliassen-Palm flux whose divergence could influence the SWJ, is weak. Secondly, the feedback of eddy heat flux on temperature field—subtropical warming, which contributes to the northward shift of SWJ, is relatively weak. On the one hand, the enhanced subtropical warming results in an enhanced poleward eddy heat flux and intensifies the indirect Ferrel cell (see Equation 10.12 and comments on Figure 10.4 in Holton, 2004). On the other hand, the intensified Ferrel cell and the associated descent in the subtropics can, in turn, exert feedback on the subtropical adiabatic warming. However, because the strength of the indirect Ferrel cell is much weaker than that of the HC, the subtropical warming induced by the feedback of eddy heat flux associated with the indirect Ferrel cell is weaker than that induced by the enhanced HC descending branch.

In essence, the jet shift is a complex nonlinear process. While EMF convergence drives the jet, the change of the jet can, in turn, influence eddy activity by changing the baroclinicity and critical latitude (Lu et al., 2008; Nie et al., 2016; Zhou et al., 2022). The mechanism linking jet, baroclinicity, and eddy activity is inherently nonlinear and complex. Any linear decomposition is an approximation and an incomplete description of the true process of jet shift. However, linear simplification does help improve our understanding of the major physical processes involved in jet shift. In a sense, the simplification is very important. For example, Rossby (1939) simplified the complex atmospheric motion and extracted the major principle that is the barotropic absolute vorticity conservation. This simplification is greatly helpful for understanding the atmospheric wave behavior. By simplifying the processes involved the jet shift, this study provides insights into the primary drivers of the northward shift of the zonal-mean SWJ, which may deepen our understanding of the jet shift.

The warming trend of sea surface temperature (SST) shows a peak over the subtropical region (Zhou et al., 2020). This SST pattern could enhance the subtropical air warming through the vertical thermal diffusion, and thus contribute to the zonal-mean northward SWJ shift. The prominent downward motion over the subtropical region (Figure 6c) would, in turn, contribute to SST warming through the adiabatic heating effect. This kind of interaction indicates that the zonal-mean SWJ shift is a complex process that involves the air-sea interaction (Yang et al., 2021), and the details about this process are worthy of investigating further. Researching on the nonlinear feedback process of jet shift is not the original intention of this paper, but it is worth conducting further in the next step.

The results of this study can be used to the emergent constraints for future projections of the SWJ shift. Using our main study results—thermal forced zonal wind associated with the subtropical warming—may help to reduce the projection uncertainty of the zonal-mean SWJ shift. We plan to do this in our next study.

Conflict of Interest

The authors declare no conflicts of interest relevant to this study.

Data Availability Statement

All the data in this paper are publicly available from the following websites: ERA5 data (Copernicus Climate Change Service, 2019a, 2019b, 2023) are from https://cds.climate.copernicus.eu/cdsapp#!/search?text=ERA5; the CMAP dataset is from https://psl.noaa.gov/data/gridded/data.cmap.html; the GPCP dataset is from https://psl.

noaa.gov/data/gridded/data.gpcp.html; the OLR dataset is from https://psl.noaa.gov/data/gridded/data.olrcdr.interp.html.

Acknowledgments
This work was financially supported by the National Natural Science Foundation of China (42288101; 42122035; 42305057), Project funded by China Postdoctoral Science Foundation (2023M733454), and the Chinese Academy of Science Special Research Assistant project (2022000242). The authors thank the reviewers for their constructive and valuable suggestions and comments, which help us to substantially improve and strengthen the paper. The authors thank Wuqiushi Yao and Shuheng Lin for their helpful suggestions.

References

Adler, R. F., Sapiano, M. R. P., Huffman, G. J., Wang, J. J., Gu, G. J., Bolvin, D., et al. (2018). The global precipitation climatology project (GPCP) monthly analysis (new version 2.3) and a review of 2017 global precipitation. *Atmosphere*, *9*(4), 138. https://doi.org/10.3390/atmos9040138

Allen, R. J., Sherwood, S. C., Norris, J. R., & Zender, C. S. (2012). Recent Northern Hemisphere tropical expansion primarily driven by black carbon and tropospheric ozone. *Nature*, *485*(7398), 350–U393. https://doi.org/10.1038/nature11097

Archer, C. L., & Caldeira, K. (2008). Historical trends in the jet streams. *Geophysical Research Letters*, *35*(8). https://doi.org/10.1029/2008gl033614

Barnes, E. A., & Polvani, L. (2013). Response of the midlatitude jets, and of their variability, to increased Greenhouse Gases in the CMIP5 models. *Journal of Climate*, *26*(18), 7117–7135. https://doi.org/10.1175/jcli-d-12-00536.1

Chen, G., & Held, I. M. (2007). Phase speed spectra and the recent poleward shift of Southern Hemisphere surface westerlies. *Geophysical Research Letters*, *34*(21). https://doi.org/10.1029/2007gl031200

Chen, G., Lu, J., & Frierson, D. M. W. (2008). Phase speed spectra and the latitude of surface westerlies: Interannual variability and global warming trend. *Journal of Climate*, *21*(22), 5942–5959. https://doi.org/10.1175/2008jcli2306.1

Chen, W., & Huang, R. H. (2002). The propagation and transport effect of planetary waves in the Northern Hemisphere winter. *Advances in Atmospheric Sciences*, *19*(6), 1113–1126. https://doi.org/10.1007/s00376-002-0069-x

Copernicus Climate Change Service. (2019a). ERA5 monthly averaged data on pressure levels from 1979 to present [Dataset]. ECMWF. https://doi.org/10.24381/CDS.6860A573

Copernicus Climate Change Service. (2019b). ERA5 monthly averaged data on single levels from 1979 to present [Dataset]. ECMWF. https://doi.org/10.24381/CDS.F17050D7

Copernicus Climate Change Service. (2023). ERA5 hourly data on pressure levels from 1979 to present [Dataset]. https://doi.org/10.24381/CDS.bd0915c6

Davis, N., & Birner, T. (2016). Climate model biases in the width of the tropical belt. *Journal of Climate*, *29*(5), 1935–1954. https://doi.org/10.1175/jcli-d-15-0336.1

Davis, N., & Birner, T. (2017). On the discrepancies in tropical belt expansion between reanalyses and climate models and among tropical belt width metrics. *Journal of Climate*, *30*(4), 1211–1231. https://doi.org/10.1175/jcli-d-16-0371.1

Dong, B. W., Sutton, R. T., Shaffrey, L., & Harvey, B. (2022). Recent decadal weakening of the summer Eurasian westerly jet attributable to anthropogenic aerosol emissions. *Nature Communications*, *13*(1), 1148. https://doi.org/10.1038/s41467-022-28816-5

Eichelberger, S. J., & Hartmann, D. L. (2007). Zonal jet structure and the leading mode of variability. *Journal of Climate*, *20*(20), 5149–5163. https://doi.org/10.1175/jcli4279.1

Fu, Q., Johanson, C. M., Wallace, J. M., & Reichler, T. (2006). Enhanced mid-latitude tropospheric warming in satellite measurements. *Science*, *312*(5777), 1179. https://doi.org/10.1126/science.1125566

Fu, Q., & Lin, P. (2011). Poleward shift of subtropical jets inferred from satellite-observed lower-stratospheric temperatures. *Journal of Climate*, *24*(21), 5597–5603. https://doi.org/10.1175/jcli-d-11-00027.1

Haynes, P. H., Marks, C. J., McIntyre, M. E., Shepherd, T. G., & Shine, K. P. (1991). On the downward control of extratropical diabatic circulations by eddy-induced mean zonal forces. *Journal of the Atmospheric Sciences*, *48*(4), 651–679. https://doi.org/10.1175/1520-0469(1991)048<0651:otcoed>2.0.co;2

Held, I. M. (2000). The general circulation of the atmosphere. In *Proceedings of Program in Geophysical Fluid dynamics* (pp. 1–36). Woods Hole Oceanographic Institution.

Hersbach, H., Bell, B., Berrisford, P., Hirahara, S., Horanyi, A., Munoz-Sabater, J., et al. (2020). The ERA5 global reanalysis. *Quarterly Journal of the Royal Meteorological Society*, *146*(730), 1999–2049. https://doi.org/10.1002/qj.3803

Holton, J. R. (2004). *An introduction to dynamic meteorology*. Elsevier.

Hu, Y., & Fu, Q. (2007). Observed poleward expansion of the Hadley circulation since 1979. *Atmospheric Chemistry and Physics*, *7*(19), 5229–5236. https://doi.org/10.5194/acp-7-5229-2007

Hu, Y. Y., Huang, H., & Zhou, C. (2018). Widening and weakening of the Hadley circulation under global warming. *Science Bulletin*, *63*(10), 640–644. https://doi.org/10.1016/j.scib.2018.04.020

Kang, S. M., Deser, C., & Polvani, L. M. (2013). Uncertainty in climate change projections of the Hadley circulation: The role of internal variability. *Journal of Climate*, *26*(19), 7541–7554. https://doi.org/10.1175/jcli-d-12-00788.1

Kang, S. M., & Lu, J. (2012). Expansion of the Hadley cell under global warming: Winter versus summer. *Journal of Climate*, *25*(24), 8387–8393. https://doi.org/10.1175/jcli-d-12-00323.1

Kushner, P. J., Held, I. M., & Delworth, T. L. (2001). Southern Hemisphere atmospheric circulation response to global warming. *Journal of Climate*, *14*(10), 2238–2249. https://doi.org/10.1175/1520-0442(2001)014<0001:shacrt>2.0.co;2

Lee, S., & Kim, H. K. (2003). The dynamical relationship between subtropical and eddy-driven jets. *Journal of the Atmospheric Sciences*, *60*(12), 1490–1503. https://doi.org/10.1175/1520-0469(2003)060<1490:tdrbsa>2.0.co;2

Liebmann, B., & Smith, C. A. (1996). Description of a complete (interpolated) outgoing longwave radiation dataset. *Bulletin of the American Meteorological Society*, *77*(6), 1275–1277.

Lorenz, D. J., & DeWeaver, E. T. (2007). Tropopause height and zonal wind response to global warming in the IPCC scenario integrations. *Journal of Geophysical Research*, *112*(D10), 11. https://doi.org/10.1029/2006jd008087

Lu, J., Chen, G., & Frierson, D. M. W. (2008). Response of the zonal mean atmospheric circulation to El Nino versus global warming. *Journal of Climate*, *21*(22), 5835–5851. https://doi.org/10.1175/2008jcli2200.1

Lu, J., Sun, L. T., Wu, Y. T., & Chen, G. (2014). The role of subtropical irreversible PV mixing in the zonal mean circulation response to global warming-like thermal forcing. *Journal of Climate*, *27*(6), 2297–2316. https://doi.org/10.1175/jcli-d-13-00372.1

Manney, G. L., & Hegglin, M. I. (2018). Seasonal and regional variations of long-term changes in upper-tropospheric jets from reanalyses. *Journal of Climate*, *31*(1), 423–448. https://doi.org/10.1175/jcli-d-17-0303.1

Menzel, M. E., Waugh, D., & Grise, K. (2019). Disconnect between Hadley cell and subtropical jet variability and response to increased CO_2. *Geophysical Research Letters*, *46*(12), 7045–7053. https://doi.org/10.1029/2019gl083345

Nie, Y., Zhang, Y., Chen, G., & Yang, X.-Q. (2016). Delineating the barotropic and baroclinic mechanisms in the midlatitude eddy-driven jet response to lower-tropospheric thermal forcing. *Journal of the Atmospheric Sciences*, *73*(1), 429–448. https://doi.org/10.1175/jas-d-15-0090.1

Panetta, R. L., & Held, I. M. (1988). Baroclinic eddy fluxes in a one-dimensional model of quasi-geostrophic turbulence. *Journal of the Atmospheric Sciences*, *45*(22), 3354–3365. https://doi.org/10.1175/1520-0469(1988)045<3354:befiao>2.0.co;2

Phillips, N. A. (1954). Energy transformations and meridional circulations associated with simple baroclinic waves in a two-level, quasi-geostrophic model. *Tellus*, *6*(3), 273–286. https://doi.org/10.1111/j.2153-3490.1954.tb01123.x

Rossby, C. G. (1939). Relation between variations in the intensity of the zonal circulation of the atmosphere and the displacements of the semipermanent centers of action. *Journal of Marine Research*, *2*(1), 38–55. https://doi.org/10.1357/002224039806649023

Vallis, G. K., Gerber, E. P., Kushner, P. J., & Cash, B. A. (2004). A mechanism and simple dynamical model of the North Atlantic Oscillation and annular modes. *Journal of the Atmospheric Sciences*, *61*(3), 264–280. https://doi.org/10.1175/1520-0469(2004)061<0264:amasdm>2.0.co;2

Vallis, G. K., Zurita-Gotor, P., Cairns, C., & Kidston, J. (2015). Response of the large-scale structure of the atmosphere to global warming. *Quarterly Journal of the Royal Meteorological Society*, *141*(690), 1479–1501. https://doi.org/10.1002/qj.2456

Waugh, D. W., Grise, K. M., Seviour, W. J. M., Davis, S. M., Davis, N., Adam, O., et al. (2018). Revisiting the relationship among metrics of tropical expansion. *Journal of Climate*, *31*(18), 7565–7581. https://doi.org/10.1175/jcli-d-18-0108.1

Williams, G. P. (1979). Planetary circulations.2. Jovian quasi-geostrophic regime. *Journal of the Atmospheric Sciences*, *36*(5), 932–968. https://doi.org/10.1175/1520-0469(1979)036<0932:pctjqg>2.0.co;2

Wu, Y. T., Seager, R., Ting, M. F., Naik, N., & Shaw, T. A. (2012). Atmospheric circulation response to an instantaneous doubling of carbon dioxide. Part I: Model experiments and transient thermal response in the troposphere. *Journal of Climate*, *25*(8), 2862–2879. https://doi.org/10.1175/jcli-d-11-00284.1

Xie, P. P., & Arkin, P. A. (1997). Global precipitation: A 17-year monthly analysis based on gauge observations, satellite estimates, and numerical model outputs. *Bulletin of the American Meteorological Society*, *78*(11), 2539–2558. https://doi.org/10.1175/1520-0477(1997)078<2539:gpayma>2.0.co;2

Yang, D. X., Arblaster, J. M., Meehl, G. A., & England, M. H. (2021). The role of coupled feedbacks in the decadal variability of the southern Hemisphere eddy-driven jet. *Journal of Geophysical Research-Atmospheres*, *126*(20). https://doi.org/10.1029/2021jd035023

Yang, H., Lohmann, G., Lu, J., Gowan, E. J., Shi, X. X., Liu, J. P., & Wang, Q. (2020). Tropical expansion driven by poleward advancing midlatitude meridional temperature gradients. *Journal of Geophysical Research-Atmospheres*, *125*(16). https://doi.org/10.1029/2020jd033158

Yang, H., Lohmann, G., Shi, X., & Muller, J. (2023). Evaluating the mechanism of tropical expansion using idealized numerical experiments. *Ocean-Land-Atmosphere Research*, *2*(0004). https://doi.org/10.34133/olar.0004

Yeh, T. C. (1957). On the formation of quasi-geostrophic motion in the atmosphere. *Journal of the Meteorological Society of Japan, The 75th Anniversary Volume*, *35A*(0), 130–134. https://doi.org/10.2151/jmsj1923.35a.0_130

Zhou, C., Lu, J., Hu, Y. Y., & Zelinka, M. D. (2020). Responses of the Hadley circulation to regional sea surface temperature changes. *Journal of Climate*, *33*(2), 429–441. https://doi.org/10.1175/jcli-d-19-0315.1

Zhou, W. Y., Leung, L. R., & Lu, J. (2022). Seasonally and regionally dependent shifts of the atmospheric westerly jets under global warming. *Journal of Climate*, *35*(16), 5433–5447. https://doi.org/10.1175/jcli-d-21-0723.1